Bioresource Technology 438 (2025) 133171

Contents lists available at ScienceDirect

Bioresource Technology

journal homepage: www.elsevier.com/locate/biortech

Metaproteomic insights into salinity's impact on carbon assimilation and polyhydroxyalkanoate production in mixed cultures of purple phototrophic bacteria☆

Jose Ramon Lorenzo-Llarena, Alba Trueba-Santiso *, Anuska Mosquera-Corral, Alba Pedrouso *

CRETUS, Department of Chemical Engineering, School of Engineering, Rua Lope Gomez de Marzoa, S/n, Universidade de Santiago de Compostela 15782 Santiago de Compostela, Galicia, Spain

HIGHLIGHTS

- Proteomics shows salinity drives microbial community and metabolic shifts.
- Salinity (35 g NaCl/L) boosts PHA production in PPB mixed cultures up to 40 dw %.
- In saline conditions, *Cereibacter* uses ethylmanonyl-CoA pathway.
- *Rhodopseudomonas* dominate the non-saline reactor with an active glyoxylate cycle.
- Salinity induces osmoprotectant (trehalose, proline, betaine) production.

GRAPHICAL ABSTRACT

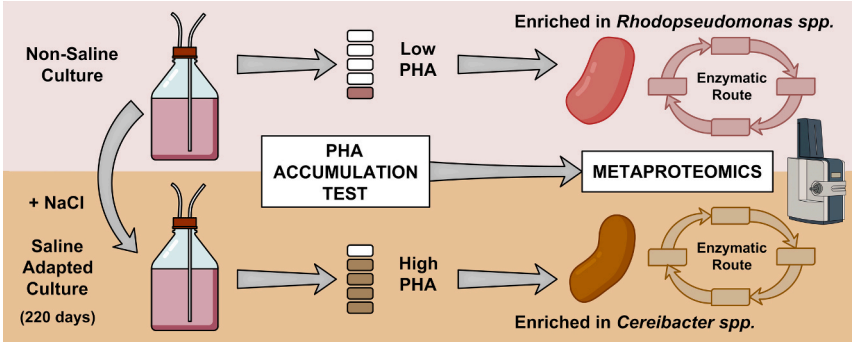

ARTICLE INFO

Keywords:
Bioreactor
Metabolic pathways
Microbial community adaptation
Photofermentation
Purple non-sulfur bacteria
Osmotic stress
Resource recovery

ABSTRACT

Purple phototrophic bacteria (PPB) are metabolically versatile microorganisms capable of adapting to diverse environmental conditions in biotechnological applications, including polyhydroxyalkanoate (PHA) production. This study explores how salinity drives metabolic specialization by comparing non-saline (R-NS) and saline-adapted (R-S) cultures fed with acetic acid. R-S accumulated significantly more PHA (up to 42 dw%) than in R-NS (up to 11%). Proteomic analyses revealed distinct communities and carbon assimilation pathways. R-NS, dominated by *Rhodopseudomonas*, relied on the glyoxylate cycle. While R-S, dominated by *Cereibacter,* employed the ethylmalonyl-CoA (EMC) pathway. EMC may provide proton motive force to support osmotic regulation in R-S, with excess reducing power equivalents stored as PHA. This is supported by glutamate synthesis overexpression and detection of osmolyte transporters. These findings underscore the adaptability of PPB to salinity, the role of reducing power in saline stress response, and suggest that the EMC pathway can sustain PHA biosynthesis even with carboxylation steps.

☆ This article is part of a special issue entitled: 'PHOTOREFINERIES 2024' published in Bioresource Technology.

* Corresponding authors.
E-mail addresses: joseramon.lorenzo.llarena@usc.es (J.R. Lorenzo-Llarena), albamaria.trueba@usc.es (A. Trueba-Santiso), anuska.mosquera@usc.es (A. Mosquera-Corral), alba.pedrouso@usc.es (A. Pedrouso).

https://doi.org/10.1016/j.biortech.2025.133171
Received 14 March 2025; Received in revised form 14 August 2025; Accepted 16 August 2025
Available online 18 August 2025

1. Introduction

Understanding how microbial communities respond to environmental stress is crucial for both ecological studies and the development of new biotechnological strategies. Purple phototrophic bacteria (PPB) are a metabolically flexible group of anoxygenic photosynthetic gram-negative prokaryotes widely found in diverse terrestrial and aquatic environments (Hunter et al., 2009).

These organisms rely on infrared light for ATP production and can alternate between autotrophic and heterotrophic growth depending on the environmental conditions (Hunter et al., 2009). This adaptability makes PPB highly promising for resource recovery and the production of value-added bioproducts. Among these, polyhydroxyalkanoates (PHAs) are one of the most notable. These biodegradable and biocompatible polyesters are typically produced by various microorganisms as a stress response to conditions such as nutrient limitation and osmotic imbalance (Carlozzi et al., 2020; Oliveira et al., 2017). Although PHAs have yet to match the cost-efficiency of petroleum-based plastics, growing legal and market demands for bio-based materials are pushing research forward (Capson-Tojo et al., 2020).

PPB light-driven ATP generation allows them to divert more organic carbon to PHA production, potentially leading to higher yields than classical PHA-accumulating aerobic cultures. However, using artificial light can raise operational costs, even when aeration is not required (Capson-Tojo et al., 2020). One way to lower costs is to use mixed microbial cultures (MMCs), which avoid the need for sterile conditions and can process waste streams directly (Oliveira et al., 2017). This approach can cut production expenses by up to 50 % (Rajendran and Han, 2022), making the use of sunlight and MMCs a promising route for PHA production with PPB.

Although MMCs introduce complexities related to community dynamics, their feasibility is evident. A systematic review of 177 studies found PHA accumulation in MMCs comparable to axenic cultures of *Cereibacter sphaeroides* (Capson-Tojo et al., 2020). In fact, using acetate under non-saline conditions, MMCs of PPB have reached PHA contents of up to 60 % of dry cell weight, with yields around 0.67 ± 0.01 Cmol PHB/Cmol acetate (Fradinho et al., 2016). Similar accumulation values have been reported for pure cultures of *C. sphaeroides F17* grown fed with the same substrate (Mugnai et al., 2025).

Salinity is a critical environmental factor influencing PHA production in microbial systems, which can affect microbial composition and shift metabolic pathways (Hülsen et al., 2019; Imhoff et al., 2020; Mosquera-Corral et al., 2021). For instance, *Rhodovulum sulfidophilum DSM-1374* produced its highest PHA content (33 ± 1.5 %) under the most saline condition tested (4.5 %) (Carlozzi et al., 2020). Similarly, mixed PPB cultures treating short-chain carboxylates under saline conditions have reached productivities like those obtained in non-saline setups (Carvalho et al., 2025). One study even reported up to 84.1 % PHA content in saline systems enriched with *Rhodobacteraceae* (Carvalho et al., 2022). Despite these promising results, the specific metabolic adaptations differentiating PPB cultures under saline versus non-saline conditions remain poorly understood. Traditional analytical approaches offer limited resolution for linking community composition with functional activity, particularly in complex mixed microbial systems.

To help close that gap, metaproteomic tools offer a way to track protein-level shifts in response to environmental changes, revealing the active metabolism of specific microbial groups within complex communities (Kleiner, 2019; Quiton-Tapia et al., 2023). However, metaproteomic data for PPB and PHA production, are still scarce. Most studies have focused on single-species systems like *Rhodospirillum rubrum S1H* (Bayon-Vicente et al., 2020), rather than mixed cultures. Understanding proteome expression shifts can provide valuable insights for optimizing PPB-based bioprocesses for enhanced PHA intracellular content. For example, Cerruti (2022) used metaproteomics to study the effect of light intensity on PPB-dominated MMCs. Under low light, phototrophic proteins were particularly abundant, and proteins related to PHA metabolism were upregulated, likely reflecting a redox imbalance.

This study aims (i) to evaluate how salinity influences PHA accumulation and bacterial main activities in mixed PPB cultures, and (ii) to explore the metabolic pathways involved in PHA synthesis under saline and non-saline conditions through metaproteomic analysis. By comparing a saline-adapted culture (R-S, 35 g NaCl/L) and a non-saline one (R-NS, 0 g NaCl/L), the goal is to identify the proteome-level shifts associated with these adaptations.

2. Material and methods

2.1. Bioreactor operation and culture acclimation

Two identical 2-liter glass bioreactors were operated in parallel in batch mode, each under a different salinity condition. The reactors were hermetically sealed and kept at room temperature (25 ± 3 °C). Anaerobic conditions were ensured by flushing each reactor with Helium for 10 min before sealing. To promote thorough mixing, the reactors were placed on magnetic stir plates at approximately 500 rpm.

Both reactors were inoculated with equal volumes (400 mL) of the same PPB-rich MMC (resulting in 150 mg VSS) and fed with identical growth media composition, except for the salinity. This MMC inoculum originated from a long-term enrichment reactor operating under non-saline conditions (R-NS), continuous illumination, and the same feeding used in the present work. Reactors were operated in cycles where the medium was refreshed with a volumetric exchange ratio of 80 % v/v every 84 h, resulting in a hydraulic retention time (HRT) of 4.4 days. The saline-adapted culture (R-S) was gradually acclimated to higher salinity by increasing NaCl concentration from 0 to 35 g/L over 8 operational cycles. The acclimation protocol involved a systematic stepwise increase of 4.4 g NaCl/L every 3.5 days, when the medium was refreshed. After acclimation, the salinity in R-S was maintained at 35 g NaCl/L.

The growth media, adapted from Ormerod et al. (1961), contained the following components in mg per liter of deionized water: 1,125 K_2HPO_4, 750 KH_2PO_4, 250 $MgSO_4$, 94 $CaCl_2{\cdot}2\ H_2O$, 14 $FeSO_4$, 25 EDTA, 25 Yeast extract as B vitamin source, and 1.25 mL/L of trace solution. The trace solution was composed (in mg/L) of: 280 H_3BO_3, 250.2 $MnCl_2{\cdot}4\ H_2O$, 75 $Na_2MoO_4{\cdot}2\ H_2O$, 20.8 $ZnCl_2$ and 4 $CuSO_4{\cdot}5\ H_2O$. Acetic acid ($C_2H_4O_2$) (488.3 g/L, 520 mg COD/L) and ammonium chloride (NH_4Cl) (106 mg N/L) were added as carbon and inorganic nitrogen sources, respectively.

Light was continuously supplied by 100 W incandescent lamps located 20 cm from the reactors. To enhance PPB competition against other phototrophic organisms, the reactors were covered with a UV/VIS absorbing foil (ecolours + e299 selector, Rosco), allowing infrared light (805–1035 nm) to pass through. An average irradiance value of 205.6 ± 12.5 W/m^2 was recorded inside the UV/VIS absorbing foil using a Hukseflux® SR05-LI19 sensor. Considering a dilution factor of 1.57 for curved surfaces (Carlozzi et al., 2020), the adjusted average irradiance decreased to 131.0 ± 7.9 W/m^2.

2.2. PHA accumulation tests

PHA accumulation tests were conducted with biomass samples collected from R-S and R-NS after 220 days (approximately 63 microbial generations) operating at stable salinities to evaluate the PHA accumulation potential of the two cultures. First, cultures were monitored over a standard growth cycle to assess PHA production under the operational feeding regime described in Section 2.1.

Next, PHA accumulation tests were carried out over 96 h under permanent feast conditions. To promote PHA storage, besides the medium fed as described in Section 2.1, two additional pulses of acetic acid (520 mg COD/L each) were added at 24 and 48 h of the cycle. This

strategy was employed to prioritize PHA accumulation over biomass growth under nutrient limitation (no ammonium was added), combined with a permanent excess carbon source (Fradinho et al., 2016). The pH of the growth medium and subsequent acetic acid pulses was adjusted to 6.5 using 1 M NaOH. Samples were taken daily throughout the 96-hour assay to monitor culture performance. A supplementary test replicated the permanent feast assay but included ammonium in the pulses to maintain the same C/N ratio as in the growth cycles.

2.3. PHA quantification

PHA content was quantified by gas chromatography (GC) following the methodology adapted from (Smolders et al., 1994). Briefly, 100 mL broth samples were taken, and 5 drops of 37 % formaldehyde were added to prevent biological activity during sample processing. Then, samples were centrifuged (Centrifuge 5430, Eppendorf, USA) and the solid phase was dried in an oven (Wulkex C-80) at 55 °C for 48 h. A known amount of dried biomass (15 – 30 mg) was placed in a tube where 50 μL of a benzoic acid solution (20 g/L) were added as internal standard, 1.5 mL of a mixture of 1-propanol and concentrated HCl (4:1) and 1.5 mL dichloromethane were added. The tubes were then heated at 100 °C for 3 h. After cooling, the organic phase was extracted with 3 mL of water and double-injected into the GC with an HP Innovax column (Agilent, USA) at 200 °C equipped with a flame ionization detector (FID) at 240 °C. PHA quantification was performed using co-polymer poly(3-hydroxybutyric acid-*co*-3-hydroxyvaleric acid) with 8 % mol of PHV content (Sigma-Aldrich) as commercial standard. PHA content was expressed as a percentage of dry weight (dw%) based on the measured volatile suspended solids (VSS). Active biomass (X_A) was estimated by assuming no other accumulation products are present; thus, by subtracting PHA mass from VSS.

2.4. Other macroscopic parameters

The pH value of raw samples was measured using a GLP 22 Crison pH meter (Spain). Total and volatile suspended solids (TSS and VSS) were determined according to Standard Methods for Water Examination (American Public Health Association, American Water Works Association, Water Environment Federation, 2023). Then, mixed liquid medium samples were centrifuged and filtered through a 0.45 μm cellulose-ester membrane filter (Advantec, Japan) for the quantification of ammonium (Bower and Holm-Hansen, 1980), and chemical oxygen demand (COD) determined according to Standard Methods for Water Examination (American Public Health Association, American Water Works Association, Water Environment Federation, 2023) for the non-saline samples. Additional $HgSO_4$ was added to the dichromate solution to prevent chloride interferences (Soto et al., 1989) for R-S samples.

2.5. Protein extractions

Samples (10 mL) were collected from each bioreactor at the start (t_0) and at 72 h (t_{72}) of the PHA accumulation cycle to perform shotgun proteomics analyses, aimed at gaining deeper insights into intracellular activities and the population dynamics involved in carbon assimilation and PHA formation. Samples were directly frozen until further proteome extraction was carried out. Protein extraction was performed following the protocol described by Quiton-Tapia et al. (2023). Briefly, samples were centrifuged at 9,000 rpm for 10 min at 4 °C to pellet the bacterial cells. Then, the pellet was washed with PBS buffer and incubated at 90 °C for 20 min in extraction buffer (50 mM Tris, 1 % SDS, pH 7.5). Cell lysis was achieved by mechanical bead beating of the obtained pellets with BeadBug™ (Merck) prefilled tubes of 2.0 mL capacity with 0.1 mm acid washed Silica glass beads in a cell disruptor (Thermo Scientific). Disruption was done in three cycles of 4 min-bead beating alternated with 1 min-incubations on ice. The lysates were then centrifuged (20 min, 3,300 rpm, 4 °C), and the supernatants were transferred to a fresh tube for protein precipitation. Two steps of −20 °C-cold acetone precipitation were performed to remove organic contaminants and salts. Then, acetone was carefully removed, and pellets were resuspended in molecular-grade water. Protein concentration was quantified using the BCA Protein Assay Kit (Thermo Fisher Scientific). Protein electrophoresis in denaturing conditions was performed with the proteome samples as quality check control in NuPAGE Bis-Tris 4–12 % gels (Thermo Fisher Scientific) at 200 V for 30 min. A standard blue Coomassie staining protocol was used for visualization of the protein bands.

2.6. Proteome analyses

Proteomic analyses were performed at the Mass Spectrometry and Proteomics facilities of the University of Santiago de Compostela (RIAIDT-USC). Protein samples were enzymatically digested and desalted using ZipTip-μC18 material (Merck Millipore, Burlington, MA). Peptides were analyzed using a nano-UHPLC-Tims-QTOF technique. Peptide samples (0.3 μg of protein) were injected into a timsTOF Pro mass spectrometer (Bruker, Bremen, Germany) equipped with a nano-electrospray source (CaptiveSpray) and a tims-QTOF analyzer.

2.7. Metaproteomic data analyses

MS/MS spectra were processed with PEAKS Studio Xpro software (Bioinformatics Solutions Inc., Waterloo, ON) for protein identification. The database used contained the sequences available in NCBI's protein database (Ma et al., 2003) for all PPBs taxonomies described in the literature in July 2023. The Label-Free and Compare modules from PEAKS Studio Xpro were used for protein quantification. Quantitative data were further processed using Python for data analyses. Proteins identified with unique peptides ≤ 1 were excluded to reduce the likelihood of false positives (Zhao and Lin, 2010). After applying this filter, relative peptide contributions were calculated for each PPB genus present in the samples. Data were grouped for genera/proteins contributing < 0.5 % to total peptides as "others".

To explore the fraction of proteins without reference information in the selected database, and therefore that were not identified in the initial round of analyses, the list of 'de novo only' peptides (i.e., sequences from MS/MS spectra that were not confidently assigned to any database peptide) was downloaded from PEAKS. The data is presented in an Excel spreadsheet as Supplementary Material. The corresponding peptides were analysed with Unipept Desktop v2.0.2. (https://unipept.ugent.be/).

The mass spectrometry proteomics data have been deposited in the ProteomeXchange Consortium via the PRIDE (Perez-Riverol et al., 2025) partner repository with the dataset identifier PXD061222.

2.8. Calculation of redox potential contribution

The standard Gibbs free energy contribution of each redox equivalent was estimated using their individual standard reduction potentials (E_0'), as reported in the literature (Berg, 2023). The energy available per molecule was calculated using the equation:

$$\Delta G^{\circ\prime} = -nFE'_0$$

where n is the number of electrons transferred (2 for both NADH and $FADH_2$), F is the Faraday constant (96.48 kJ/(mol·V)), and E_0' is the standard reduction potential: (−0.32 V for NADH and −0.22 V for $FADH_2$) yielding + 61.75 kJ/mol and + 42.45 kJ/mol, respectively. The total ΔG°' was obtained by multiplying these values by the net production or consumption of each redox equivalent in the metabolic pathways identified through proteomic analysis.

3. Results and discussion

3.1. Characterization of polyhydroxyalkanoate accumulation assays

With the biomass collected from the batch reactors R-S and R-NS, PHA accumulation tests were conducted to highlight the primary metabolic differences between the two PPB enriched mix cultures in absence and presence of saline conditions, respectively (Fig. 1). After 72 h (t_{72}), R-NS culture exhibited limited PHA accumulation (11 dw%) with a carbon yield of only 0.05 Cmol/Cmol based on the consumed substrate, and a productivity of 0.80 Cmmol-PHA/(L·d). In contrast, the R-S culture demonstrated significantly higher PHA accumulation, reaching 33 dw%, with a carbon yield of 0.18 Cmol/Cmol and productivity of 1.32 Cmmol-PHA/(L·d). In both systems, PHA was predominantly composed of polyhydroxybutyrate (PHB) (Fig. 1), which aligns with the literature, particularly when acetic acid (C_2) serves as the main carbon source (Yuan et al., 2015).

A follow-up PHA assay performed 24 h later (t_{96}) revealed further metabolic disparities. While R-S continued accumulating PHA, reaching 42 dw%, R-NS consumed nearly 50 % of its stored PHA (Fig. 1). This trend was also reflected in the carbon conversion efficiency: the carbon yield of PHA from substrate consumed in R-S increased to 0.25 Cmol/Cmol, while in R-NS it decreased sharply to 0.03 Cmol/Cmol. Similarly, PHA productivity rose to 1.86 Cmmol-PHA/(L·d) but dropped to 0.34 Cmmol-PHA/(L·d) in R-NS.

These differences were reflected in distinct COD consumption patterns (see supplementary material, Fig. S1). R-NS showed higher COD consumption rates, leaving 150 mg COD/L at 72 h and further depleting it at t_{96}, forcing the cells to degrade PHA for energy. Conversely, R-S exhibited slower kinetics (800 mg COD/L remaining at t_{72}). At 72 h, R-NS had twice the active biomass (0.58 g X_A/L) of R-S (0.23 g X_A/L), accompanied by double nitrogen (which was never limited, see supplementary material, Fig. S1) assimilation. This suggests that saline conditions promote metabolic pathways favoring PHA synthesis rather than growth. The trend of higher PHA accumulation in the saline-adapted reactor was also observed in additional tests performed with R-NS and R-S cultures (see supplementary material, Fig. S2). Although not accompanied by metaproteomic analysis, these tests further support the robustness of the observed pattern.

Under saline conditions (45 g NaCl/L), similar PHA accumulation values have been observed when working with a pure culture of *Rhodovulum sulfidophilum* DSM-1374, reaching 33.0 ± 1.5 % PHB content fed with lactate (Carlozzi et al., 2020). However, it is important to note that in the present study, the PHA accumulation values are not the maximum achievable, as the biomass was not previously enriched for PHA accumulation and carbon pulses were not maximized. A previous study, under non saline conditions, reported PHA contents up to 60 dw% under a light intensity of 227 W/m^2, utilizing previously enriched biomass in permanent feast conditions fed with an organic loading rate (OLR) of 1.3 g COD/(L·d) (Fradinho et al., 2016), which is significantly higher than the 0.15 g COD/(L·d) applied in R-S and R-NS.

3.2. Metaproteomics

A total of 27,214 (t_0) and 27,854 (t_{72}) peptides were detected in R-S, and 10,641 (t_0) and 15,110 (t_{72}) in R-NS samples. This resulted in the identification of 6187, 6433, 3097, and 4038 proteins, respectively, through PEAKS software analyses and using a custom database constructed by downloading all the aminoacidic sequences available on NCBI and belonging to a total of 49 PPB genera. The 'de novo only' list generated on the PEAKS analyses was also evaluated (see supplementary material) and contained 128 (R-S t_0), 137 (R-S t_{72}), 308 (R-NS t_0), and 189 (R-NS t_{72}) peptides, respectively, indicating that proteins without reference in the applied database can be considered a minority.

3.3. Composition of the active microbial community under non-saline and saline conditions

Relative peptide contributions of PPB genera showed that salinity drives significant shifts in the active microbial community composition, as observed in samples collected in the accumulation experiments at t_0 (Fig. 2).

A total of 41 and 40 PPB genera were detected at time 0 and 72 h on R-S, and 37 and 44 PPB genera at time 0 and 72 h on R-NS. Among PPB, both reactors were enriched with purple non-sulfur bacteria (PNSB), while purple sulfur bacteria (PSB) were nearly absent, with their proteins accounting for 0.75 % and 0.3 % of the total PPB biomass in R-NS and R-S, respectively. The limited presence of PSB (mainly from *Chromatiaceae* family) aligns with their preference for photoautotrophic growth (Hunter et al., 2009), whereas acetate was the carbon source used in this study.

In R-NS, the active community was primarily composed of members from the families *Nitrobacteraceae,* (a 75.5 %, contribution from the genus *Rhodopseudomonas*), with *Rhodopseudomonas palustris* accounting for approximately 57 %. Other relevant genera include *Rhodoferax* (14.8 %, from the *Comamonadaceae* family) and *Rubrivivax* (3.9 % from the *Sphaerotilaceae* family). In contrast, salinity led to a strong dominance of the *Rhodobacteraceae* family (> 97 %), with *Cereibacter* (68.6 %) and *Rhodobacter* (14.6 %) as the most abundant genera.

The dominant species in R-S, *Cereibacter sphaeroides* (68.6 % peptide contribution), was previously classified as *Rhodobacter sphaeroides* but was reassigned to the *Cereibacter* genus during a taxonomic

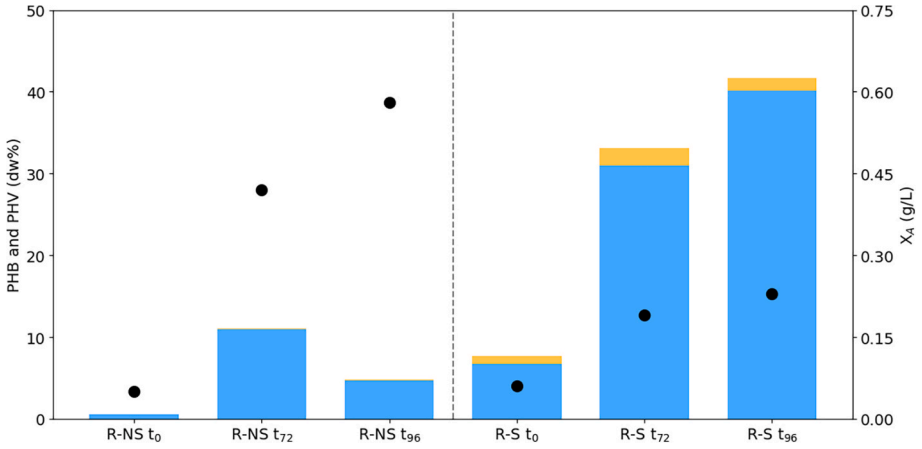

Fig. 1. Evolution of the percentage of polyhydroxybutyrate (PHB) (□) and polyhydroxyvalerate (PHV) (□) accumulated intracellularly during the polyhydroxyalkanoate accumulation tests, expressed as a percentage of the total biomass dry weight (dw%) and concentration of active biomass (XA) in g/L.

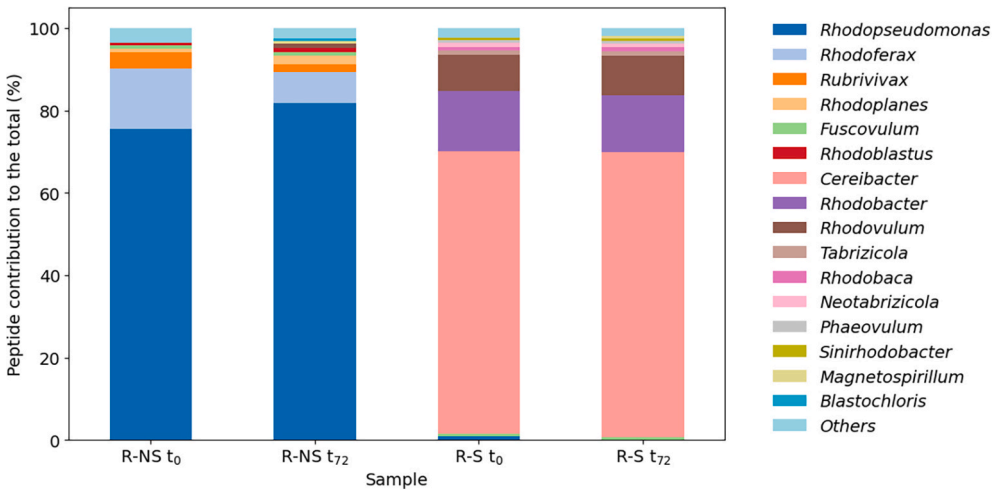

Fig. 2. Peptide relative contributions of each bacterial genus (≥ 0.5 %) to the total peptide number identified in each sample from the non-saline (R-NS) and saline (R-S) bioreactors at the initial time (t_0) and after 72 h (t_{72}). Three independent proteome extractions from 10-mL aliquots were performed from each 2-L bioreactor at each sampling time. Proteome samples were pooled before the metaproteomic analyses.

reclassification (Hiraishi and Ueda, 1994; Hördt et al., 2020). *Cereibacter* presence in the saline R-S environment might be attributed to its demonstrated halotolerance under both laboratory (Xu et al., 1998) and natural environments, as it has been found in rice crops with saline intrusions in Vietnam (Dat et al., 2024). Recent genomic studies of *C. sphaeroides* strains S3W10 and SS15 have identified specific genes related to osmotic stress tolerance (Klaysubun et al., 2024), which likely contribute to the species' survival and proliferation in R-S.

A major morphological difference between both mixed cultures may lie in membrane structures. The *Rhodobacter* genus was established by Imhoff et al. (1984) to reclassify bacteria possessing vesicular intracytoplasmic membranes, which provide significant advantages for energy transduction processes (Niederman, 2006). A decade later, Hiraishi and Ueda (1994), proposed further differentiation within *Rhodobacter* based on their salt requirements for optimal growth. The *Rhodovulum* genus emerged from this reclassification to group the marine species. Hülsen et al. (2019) reported the progressive dominance of *Rhodovulum* over typical freshwater genera, such as *Rhodobacter*, when treating domestic wastewater under saline conditions (26 g NaCl/L). In the current study, *Rhodovulum* was the third most abundant genus in R-S (35 g NaCl/L) but did not surpass *Cereibacter* (Fig. 2).

Although halophilic PPB such as *Rhodospirillum, Chromatium, Thiocapsa,* and *Ectothiorhodospira* (Imhoff, 2001; Ollivier et al., 1994) have been described; their contribution in R-S was below 0.15 %, probably since most of them prefer photoautotrophic conditions (Hunter et al., 2009).

When comparing the community composition between the beginning (t_0) and after 72 h (t_{72}), no significant changes were observed in R-S. This suggests that the operational conditions during the PHA accumulation assay did not further alter the active community, and its structure was mainly driven by the presence or absence of salt. In R-NS, *Rhodopseudomonas* increased from 75.5 % to 81.8 %, while *Rhodopherax* contribution was reduced by half (to 7.5 %) (Fig. 2). These shifts may reflect adaptation to the changing metabolic demands of the system throughout the accumulation process.

3.4. Regulation of polyhydroxyalkanoate biosynthesis

3.4.1. Key enzymes in polyhydroxyalkanoate formation metabolic pathways

The production of PHA involves three key enzymes. Acetyl-CoA acetyltransferase (PhaA) catalyzes the condensation of two acetyl-CoA molecules (each containing two carbon atoms) to produce acetoacetyl-CoA, a four-carbon compound, liberating coenzyme A (CoA) in the process. NADPH-dependent acetoacetyl-CoA reductase (PhaB) then reduces acetoacetyl-CoA to 3-hydroxybutyryl-CoA, utilizing reducing power in the form of NADPH. Finally, polyhydroxyalkanoate synthase (PhaC) polymerizes the monomers to form the final polymer (Sagong et al., 2018) (Fig. 3). PhaC plays a crucial role in determining both the molecular weight and monomer composition of PHAs (Sagong et al., 2018) and thus, it is considered a key biomarker for PHA production. All three enzymes were significantly upregulated in R-S at the beginning and final samples of the accumulation test, whereas in R-NS, only PhaA and PhaB were identified (Fig. 3). While PhaC was not detected in R-NS, PHA production was observed (Fig. 1), suggesting either low expression below the detection limit or that PHA synthesis occurred at a different time point than sampling.

In R-NS, PHA-related enzymes were almost exclusively found in the *Rhodopseudomonas* genus. In contrast, R-S exhibited a more diverse PHA production microbial community, dominated by *Cereibacter, Rhodovulum,* and *Rhodobacter*. Although *Rhodovulum* was the third-most abundant genus in R-S (Fig. 2), it contributed twice as many peptides related to PHA metabolism compared to *Rhodobacter*. Additionally, *Neotabrizicola, Tabrizicola* or *Sinirhodobacter* (also belonging to the *Rhodobacteraceae* family) showed upregulation of PHA-related enzymes at t_{72}, highlighting their potential role in PHA metabolism under saline conditions.

3.4.2. Polyhydroxyvalerate biosynthesis limitation

Polyhydryoxyvalerate (PHV) synthesis was low (Fig. 1), likely because acetic acid (C_2) was the only carbon source fed into the system. This molecule typically leads to the production of PHB, a polymer with even-numbered carbon chains. However, the formation of odd-chain polymers, such as PHV, is still possible through metabolic routes that generate propionyl-CoA, an odd-chain intermediate. Pathways such as ethylmalonyl-CoA (EMC) pathway (Fig. 3), methyl aspartate cycle or the 3-hydroxy propionate cycle (Erb et al., 2007; Petushkova et al., 2021) can introduce propionyl-CoA into the PHA formation pathway.

In this process, PhaA enzyme catalyses the condensation of propionyl-CoA (C_3) and acetyl-CoA (C_2) to form 3-ketovaleryl-CoA (C_5). This intermediate is then reduced by PhaB, using NADPH, to 3-hydroxyvaleryl-CoA (C_5). Finally, the PhaC polymerizes 3-hydroxyvaleryl-CoA monomers into PHV (Slater et al., 1998). Notably, PHV was found mainly in R-S, reaching up to 2.1 dw%, while its maximum accumulation in R-NS was only 0.1 dw% (Fig. 2). This significantly higher PHV content in R-S, despite acetate being the sole carbon source, suggests a

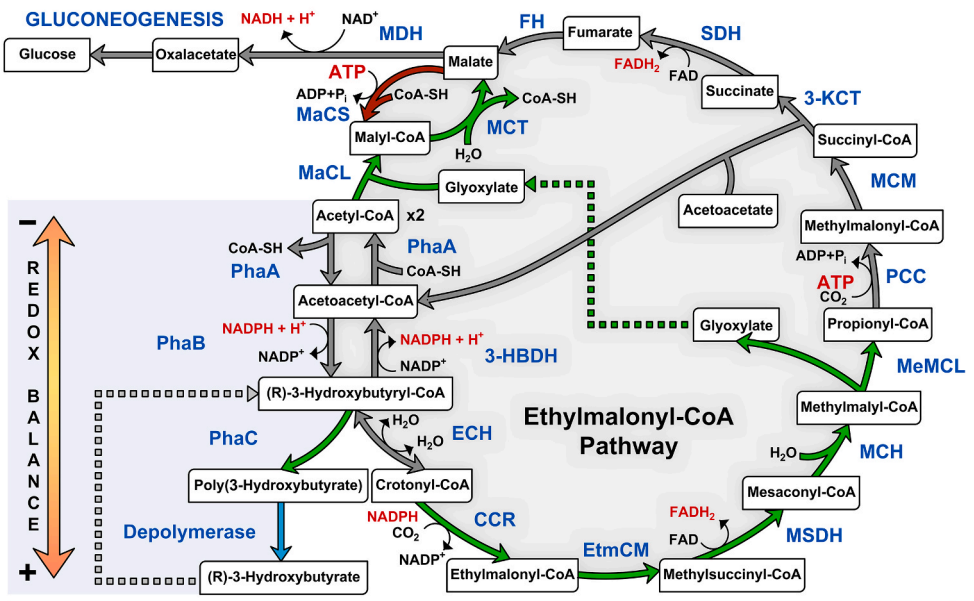

Enzymes	Gene	R-NS t_0	R-NS t_{72}	R-S t_0	R-S t_{72}
PHA Formation					
Acetyl-CoA acetyltransferase	*PhaA*	30	47	64	35
Acetoacetyl-CoA reductase	*PhaB*	20	18	15	17
Polyhydroxyalkanoate synthase	*PhaC*	0	0	22	16
Poly(3-hydroxybutyrate) depolymerase	*PhaZ*	0	10	0	0
Phasin	*PhaP*	5	62	51	122
Regulator protein	*PhaR*	43	87	10	19
Ethylmalonyl-CoA Pathway					
3-hydroxybutyryl-CoA dehydrogenase	*3-HBDH*	29	29	13	22
Enoyl-CoA hydratase	*ECH*	49	64	140	48
Crotonyl-CoA reductase	*CCR*	0	0	22	0
Ethylmalonyl-CoA mutase	*EtmCM*	0	0	32	51
Methylsuccinyl-CoA dehydrogenase	*MSDH*	0	0	16	75
Mesaconyl-CoA hydratase	*MCH*	0	0	10	12
Methylmalyl-CoA lyase	*MeMCL*	0	0	28	30
Propionyl-CoA carboxylase	*PCC*	50	158	183	112
Methylmalonyl-CoA mutase	*MCM*	0	11	87	88
3-ketoacid-CoA transferase	*3-KCT*	0	19	0	19
Malyl-CoA lyase	*MaCL*	0	0	28	83
Malyl-CoA thioesterase	*MCT*	0	0	4	38
Malyl-CoA synthase	*MaCS*	0	0	0	0

Fig. 3. Comparative polyhydroxyalkanoate (PHA) formation and ethylmalonyl-CoA Cycle pathways. Arrows represent potential enzyme presence: blue for non-saline reactor (R-NS) only, green for saline reactor (R-S) only, grey for both populations, and red for undetected enzymes. Enzyme names, abbreviations, and peptide counts are shown below the figure, with a heatmap highlighting relative abundance differences. (For interpretation of the references to colour in this figure legend, the reader is referred to the web version of this article.)

differential activation or upregulation of propionyl-CoA generating pathways, such as EMC pathway, under saline conditions (Fig. 3). The EMC pathway will be discussed in section 3.5.1.

3.4.3. Activation of depolymerase enzymes

PHA depolymerization is catalyzed by specialized depolymerase enzymes (PhaZ), which break PHA down into monomers. 3-Hydroxybutyryl-CoA monomers can either enter the EMC pathway or be converted back to acetoacetyl-CoA by 3-hydroxybutyryl-CoA dehydrogenase (3-HBDH). This reaction, which might occur under substrate limitation, generates reducing power and ultimately produces two molecules of acetyl-CoA while utilizing a free CoA.

Depolymerase enzymes were detected exclusively in R-NS, which aligns with the observed reduction in PHA content after 24 h of the second proteomic sampling (t_{72}) (Fig. 1). This observation suggests that PHA catabolism was actively occurring in the R-NS reactor to sustain biomass growth. In contrast, PHA content increased in R-S during the same period, consistent with the absence of depolymerase activity.

These enzymes in R-NS exclusively belong to the *Rhodopseudomonas* genus. This fact, combined with COD limitation (see supplementary material, Fig. S1), meant that only those capable of accumulating PHA could grow, which explains their increased relative abundance from t_0 and t_{72} (Fig. 2).

3.4.4. Phasins and PhaR enzymes in PHA regulation

Phasins (PhaP) are the major proteins associated with PHA granules,

known to promote bacterial growth and PHA synthesis as well as influence the size, number, and distribution of the PHA granules. Previous studies have shown that the cellular concentration of PhaP correlates with PHA content (Liu et al., 2022). In the present study, PhaP were detected in the R-S samples, with increased expression observed at t_{72}. On the other hand, repressor (PhaR) enzymes, which regulate PhaP and mediate PHA synthesis (Maehara et al., 2002), were present in both reactors but in higher abundance in R-NS, which might explain why PhaC enzyme was not found active in this reactor.

3.5. Comparative carbon assimilation metabolisms in saline and non-saline cultures

3.5.1. Ethylmalonyl-CoA pathway activation under saline conditions

The ethylmalonyl-CoA pathway (EMC) has been described as a key mechanism for carbon uptake in certain PPB species that allow them to convert acetate into cell biomass while avoiding unnecessary consumption of CO_2 (Bayon-Vicente et al., 2020) (Fig. 3). This pathway and PHA biosynthesis are interconnected through shared carbon intermediates as both rely on the conversion of two molecules of acetyl-CoA into acetoacetyl-CoA, catalyzed by the enzyme PhaA. From this step onwards, clear differences in enzyme expression can be observed between R-NS and R-S (Fig. 3).

R-S followed the subsequent steps of the EMC pathway (carried out by bacteria from different genera: *Cereibacter, Rhodobacter, Rhodovulum, Rhodobaca, and Neotabrizicola),* which starts by producing ethylmalonyl-CoA (C_5) by the enzyme crotonyl-CoA carboxylase/reductase (CCR) through the incorporation of CO_2. After undergoing further modifications, the compound is converted to mesaconyl-CoA, which is then cleaved into glyoxylate (C_2) and propionyl-CoA (C_3) by methylmalyl-CoA lyase (MeMCL) (Erb et al., 2007). The glyoxylate generated by MeMCL is transformed into malyl-CoA via the addition of an acetyl-CoA by malyl-CoA lyase (MaCL) and subsequently converted into malate by malyl-CoA thioesterase (MCT), a step that liberates CoA. These metabolic steps in which reducing equivalents are consumed (NADPH/NADH) and produced ($FADH_2$) were found only in R-S, while none of these enzymes were detected in R-NS.

On the other hand, propionyl-CoA is carboxylated with CO_2 by propionyl-CoA carboxylase (PCC) to form methylmalonyl-CoA (C_4), which is further modified to succinyl-CoA (Erb et al., 2007). The enzyme 3-ketoacid-CoA transferase (3-KCT) catalyzes the transfer of CoA from succinyl-CoA (the donor) to acetoacetate (the acceptor), producing succinate and acetoacetatyl-CoA (Tammam et al., 2007). This part of the metabolism was detected in both bioreactors. PCC enzymes were detected in R-NS, indicating the presence of propionyl-CoA, which may have been generated through alternative pathways such as the methylaspartate cycle or the 3-hydroxypropionate cycle (Petushkova et al., 2021).

This EMC specialization in R-S might be attributed to the long-term cultivation of the culture with acetic acid as the sole carbon source. Bayon-Vicente et al. (2020) have found an amplification of the genomic region belonging to EMC pathway after long-term cultivation of *Rhodospirillum rubrum* using acetate. In the present study, only a few enzymes associated with *R. rubrum* were detected in R-S, likely because this species requires bicarbonate in the medium to activate the EMC pathway, as noted by Bayon-Vicente et al. (2020).

3.5.2. Glyoxylate cycle dominance in carbon conservation in non-saline conditions

Glyoxylate cycle, together with the EMC, is known as carbon conservation metabolism when PPB are fed with acetate, having a key role in anaplerosis, replenishing metabolic intermediates. Glyoxylate pathway allows PPB to conserve carbon by bypassing the decarboxylation steps of the tricarboxylic acid (TCA) cycle, which otherwise leads to carbon loss as CO_2.

The glyoxylate shunt requires two molecules of acetyl-CoA. The first condenses with oxaloacetate to form citrate, which is later converted into glyoxylate and succinate. The second acetyl-CoA is combined with glyoxylate to produce malate, which is subsequently oxidized to regenerate oxaloacetate, yielding one NADH. Further oxidation of succinate through steps shared with the TCA cycle produces one $FADH_2$ and an additional NADH (See Fig. 4).

The TCA cycle is central to carbon metabolism in most bacterial taxa. This pathway facilitates the catabolism of carbon substrates by oxidizing acetyl-CoA, resulting in the production of reducing power (NADH and $FADH_2$) and energy as ATP (Fig. 4) (Petushkova et al., 2021). These products drive cellular energy requirements and support the subsequent utilization of oxaloacetate for gluconeogenesis. However, proteomic data analyses indicated partial expression of TCA cycle enzymes as succinate-CoA synthetase (SCS), the enzyme responsible for the substrate-level phosphorylation of ADP to ATP, was not detected in either reactor (Fig. 4). This absence suggests potential reliance on alternative ATP generation pathways, such as cyclic photophosphorylation, though more research is needed to confirm it.

If glyoxylate cycle is active, the ATP required for this process can theoretically be supplied through cyclic photophosphorylation, enabling PPB to avoid exclusive reliance on the TCA cycle for energy production (Eprintsev et al., 2008).

Metaproteomic analysis of R-NS revealed the presence of isocitrate lyase (ICL) and malate synthase (MS), the key enzymes of the glyoxylate cycle, indicating its activation. In contrast, R-S biomass lacked both ICL and MS, confirming the dominance of the EMC pathway in this culture (Fig. 4). This observation aligns with previous reports that *Cereibacter sphaeroides* lacks ICL (Alber et al., 2006), explaining why R-S biomass is unable to activate the glyoxylate cycle and therefore has upregulated the enzymes from the EMC pathway.

Rhodobacter capsulatus, the prevalent species of the second most abundant genus in R-S, is known to be able to utilize the glyoxylate shunt (Petushkova and Tsygankov, 2017). Nevertheless, this pathway was not active under the imposed saline conditions. Saline environments could exert selective pressures that limit the activation of specific metabolic pathways, including the glyoxylate shunt.

Shi et al., (2024) have shown that a decrease in salinity downregulates the expression of isocitrate dehydrogenase (IDH) in algae, diverting the carbon flow from isocitrate to glyoxylate. A similar behavior might occur in PPB under non-saline conditions, facilitating the activation of the glyoxylate cycle. To the authors' knowledge, this phenomenon has not been described in PPB-related literature.

3.5.3. Calvin-Benson-Bassham cycle

Calvin-Benson-Bassham (CBB) cycle uses ATP and NADPH produced in the light reactions of photosynthesis to convert CO_2 (generally produced in the TCA cycle) into glyceraldehyde-3-phosphate (G3P), which can then be used to synthesize glucose and other carbohydrates.

This cycle is facilitated by three enzymes: ribulose bisphosphate carboxylase/oxygenase (RuBisCO), phosphoglycerate kinase (PGK), and glyceraldehyde-3-phosphate dehydrogenase (GAPDH) which uses NADPH, serving as a sink for reducing equivalents (McKinlay and Harwood, 2010). All three enzymes were detected in both reactors, indicating that CO_2 was recycled through the CBB cycle (Fig. 4). PGK was not identified in R-S when the unique peptides > 1 filter was applied, although several of these enzymes were detected with only one unique peptide.

3.6. Adaptative mechanisms of osmotic stress response in PPB

3.6.1. Salt-induced stress proteins

Stress-related proteins were detected in both reactors, with total abundance at t_0 twice as high in R-S as in R-NS but ending with similar values at t_{72} (Fig. 5). In the R-NS, universal stress proteins from *Rhodopseudomonas* (accounting 95 % at t_{72}) and *Fuscovulum* were detected, likely explaining why both genera became more abundant by the end of

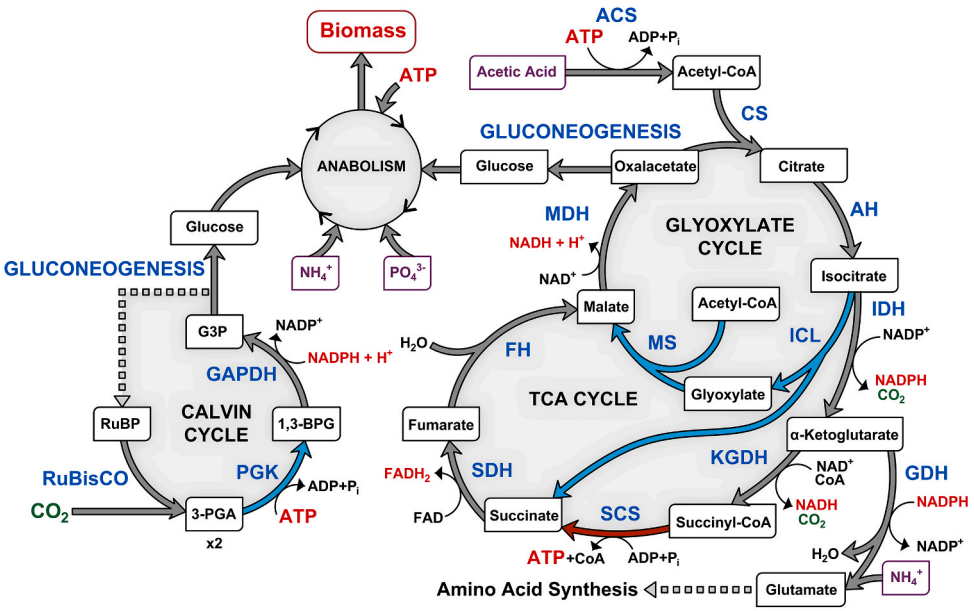

Enzymes	Gene	R-NS t_0	R-NS t_{72}	R-S t_0	R-S t_{72}
TCA Cycle					
Citrate synthase	*CS*	25	44	68	53
Aconitate hydratase	*AH*	29	11	121	86
Isocitrate dehydrogenase	*IDH*	0	127	340	235
α-ketoglurate dehydrogenase	*KGDH*	41	127	99	114
Succinyl-CoA synthetase	*SCS*	0	0	0	0
Succinate dehydrogenase	*SDH*	44	100	75	95
Fumarate hydratase	*FH*	7	3	121	135
Malate dehydrogenase	*MDH*	94	108	142	147
Amino Acid Synthesis					
Glutamate dehydrogenase	*GDH*	15	14	125	88
Glyoxylate Cycle					
Isocitrate lyase	*ICL*	95	41	0	0
Malate synthase	*MS*	16	59	0	0
Calvin-Benson-Bassham Cycle					
Ribulose bisphosphate carboxylase/oxygenase	*RuBisCO*	4	5	13	2
Phosphoglycerate kinase	*PGK*	22	21	0	0
Glyceraldehyde-3-phosphate dehydrogenase	*GAPDH*	6	0	143	78

Fig. 4. Comparative tricarboxylic acid (TCA), glyoxylate, and Calvin cycle analyses. Arrows represent potential enzyme presence: blue for enzymes in non-saline reactor (R-NS) only, blue for both populations (R-NS and saline reactor (R-S)) populations, red for undetected enzymes. Enzyme names, abbreviations, and peptide counts are shown below, with a heatmap highlighting relative abundance differences. (For interpretation of the references to colour in this figure legend, the reader is referred to the web version of this article.)

the operation (Fig. 2). The increase in stress-related proteins at the end of the PHA accumulation test can be attributed to the COD limitation (see Supplementary material, Fig. S1). In R-S universal stress proteins belong to *Rhodovulum* (77 % and 44 % at t_0 and t_{72}, respectively) and *Cereibacter*.

Moreover, specific salt-stress-induced proteins were only detected in the R-S samples, all belonging to *Cereibacter* genus, specifically *Cereibacter sphaeroides*.

3.6.2. *Glutamate role in maintaining cellular homeostasis*

Salinity stress is widely associated with the biosynthesis of intracellular osmolytes, also known as compatible solutes, that counteract osmotic pressure and maintain cellular homeostasis by preventing the inactivation, inhibition, and denaturation of macromolecules (Imhoff et al., 2020; Tsuzuki et al., 2011; Xu et al., 1998).

The role of glutamate as a key molecule in halotolerance has been widely discussed. This molecule works both as a precursor of compatible solutes such as proline and trehalose and as a non-toxic counterion of K^+. Glutamate is formed by glutamate dehydrogenase enzyme (GDH), using α-ketoglutarate as an intermediate of TCA. Its formation requires NADPH and a prior decarboxylation of isocitrate, losing CO_2.

Isocitrate dehydrogenase (IDH) enzyme was detected, likely due to its crucial role in producing α-ketoglutarate, which is necessary for glutamate production using glutamate dehydrogenase (GDH) enzyme. Both enzymes were more abundant in R-S than in R-NS (Fig. 4). GDH enzyme was present in both reactors, however, when it comes to peptide count, it was about 7 times higher in R-S than in R-NS confirming that glutamate was being synthesized as a mechanism to cope with salinity (Fig. 5). In both cultures, pyrroline-5-carboxylate reductase (P5CR) was found. This enzyme catalyzes the conversion of glutamate to proline

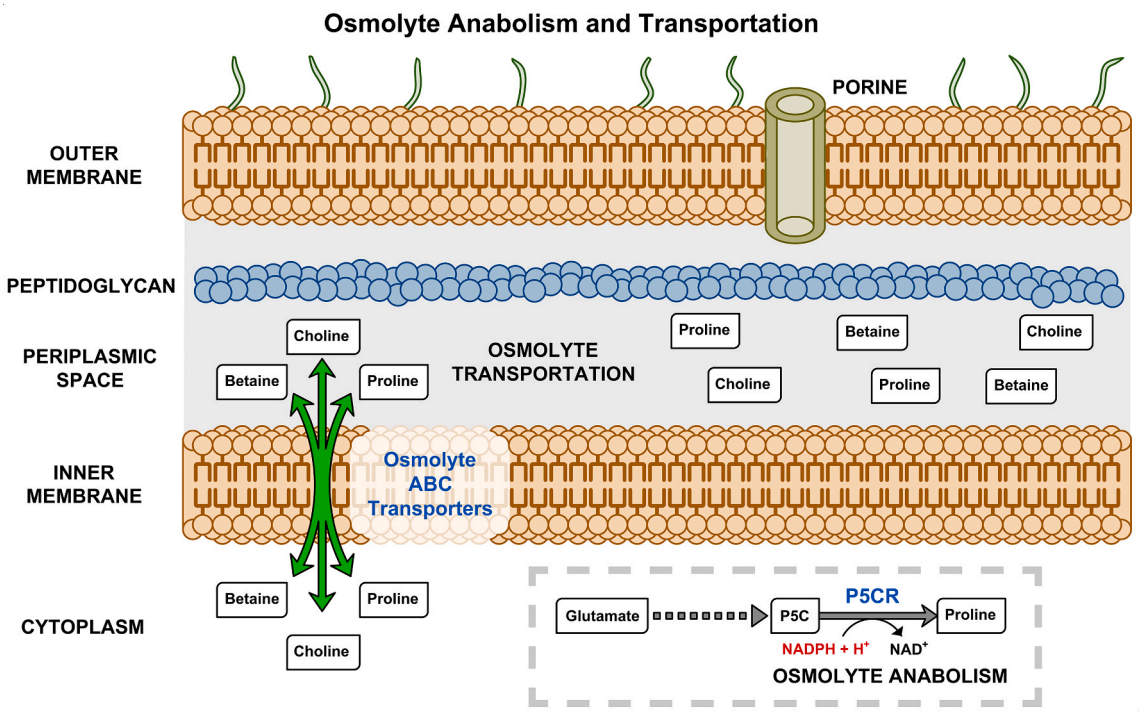

Enzymes	Gene	R-NS t_0	R-NS t_{72}	R-S t_0	R-S t_{72}
Osmolyte Anabolism and Transportation					
Osmolyte ABC transporters	-	0	0	17	24
Pyrroline-5-carboxylate reductase	*P5CR*	2	2	4	4
Trehalose-6-phosphate synthase	*TPS*	0	0	47	27
Salt Stress Protein					
Salt-stress induced outer membrane protein	*SspA*	0	0	19	25

Fig. 5. Comparative osmolyte anabolism and transportation analysis in R-NS and R-S bacterial populations. Arrows represent potential enzyme presence: grey for enzymes in both populations and green for R-S only. Enzyme names, abbreviations, and peptide counts are shown below, with a heatmap highlighting relative abundance differences. (For interpretation of the references to colour in this figure legend, the reader is referred to the web version of this article.)

(Pérez-Arellano et al., 2010) (Fig. 5). However, only in R-S culture trehalose-6-phosphate synthase enzyme was detected, which is involved in the production of trehalose, a sugar that helps maintain osmotic stress balance (Imhoff et al., 2020).

Similarly, transporter enzymes related to the biosynthesis of proline, trehalose, choline and betaine were found exclusively in the R-S culture, indicating an active response to counteract osmotic stress by accumulating compatible solutes. This reflects the ability of PPB to adjust their metabolic activities to environmental challenges (Fig. 5). Tsuzuki et al. (2011) observed rapid exogenous glycine and betaine transport (thermodynamically favored over biosynthesis (Imhoff et al., 2020) upon salt exposure in *C. sphaeroides* with trehalose as the main osmoprotectant produced. Xu et al. (1998) already reported trehalose as the main organic osmoprotectant in *C. sphaeroides denitrificants,* with its concentration varying with external salt concentration, while levels of betaine and proline did not change when osmolarity increased. Imhoff et al. (2020) reported betaine as the major compatible solute at moderate-high salinity in most PPB (including *C. sphaeroides*) but did not consider trehalose. The present study's findings support this and further suggest a broader strategy involving multiple compatible solutes in *C. sphaeroides* under high salinity (35 g NaCl/L).

3.7. Glyoxylate cycle vs. ethylmalonyl-CoA for carbon preservation

The main difference in carbon assimilation metabolism between R-NS and R-S lies in the pathway used for carbon preservation. R-NS, dominated by *Rhodopseudomonas,* relies on the glyoxylate shunt, a much simpler mechanism than EMC, that neither produces nor consumes ATP, avoids CO_2 losses, and produces 1 NADH and 0.5 $FADH_2$ per acetyl-CoA (82.97 kJ/mol) (See Table 1).

EMC pathway has been generally described as an electron sink mechanism, however, if no inorganic carbon is fed, an acetyl-CoA must be metabolized by the TCA cycle to decarboxylate two molecules of CO_2, which are later used by CCR and PCC enzymes in EMC. This likely explains the co-occurrence of IDH (isocitrate dehydrogenase) and KGDH (α-ketoglutarate dehydrogenase) enzymes in conjunction with this pathway (Figs. 3 and 4).

For this process to be fully carried out, four acetyl-CoA molecules are needed: one for the TCA cycle to supply CO_2, two for EMC, and one for converting glyoxylate to malate. The overall process produces 3 NAD(P)H, and 3 $FADH_2$ molecules, yielding 78.15 kJ/mol per acetyl-CoA. Almost the same reductive power as the glyoxylate cycle. This might suggest that EMC does not work as an electron sink if no inorganic carbon is fed. On the other hand, the lost ATP can be a significant constraint for many microorganisms. However, PPB, as photosynthetic microorganisms, gain ATP from light, making this strategy viable.

Table 1
Comparative analysis of redox balance and carbon flux in different metabolic pathways under saline and non-saline conditions. The upper section compares the glyoxylate shunt with the combination of the tricarboxylic acid (TCA) and ethylmalonyl-CoA (EMC) pathway. The lower section evaluates carbon recovery strategies following glutamate-associated decarboxylation, involving the Calvin Cycle + Glyoxylate cycle and EMC. Both panels summarize key metabolic parameters, including acetyl-CoA utilization, net CO_2 and ATP balance, redox equivalents, and standard Gibbs free energy ($\Delta G^{\circ\prime}$) derived from net redox cofactor production.

Culture	Pathway	Acetyl-CoA > Used	Net > CO_2	Net > ATP	NAD(P)H > Produced	NAD(P)H > Consumed	Net > NAD(P)H	$FADH_2$ > Produced	$\Delta G^{\circ\prime}$ > (kJ/mol)	$\Delta G^{\circ\prime}$ per > Acetyl-CoA
Glyoxylate shunt vs. TCA + EMC										
R-NS	Glyoxylate Shunt	2	0	**0**	2	0	+2	1	166.0	**83.0**
	TOTAL	2	0	**0**	2	0	+2	1	166.0	**83.0**
R-S	TCA	1	−2	**+1**	3	0	+3	1	227.7	**227.7**
	EMC	2	+2	**−1**	1	2	−1	2	23.3	**11.6**
	Glyoxylate Utilization	1	0	**0**	1	0	1	0	61.8	**61.8**
	TOTAL	4	0	**0**	5	2	+3	3	312.6	**78.2**
Carbon recovery following glutamate-associated decarboxylation										
R-NS	Glutamate Synthesis (X2)	2	−2	**0**	2	2	0	0	0.0	**0.0**
	Calvin Cycle (X2)	0	+2	**−6**	0	4	−4	0	−247.0	**N/A**
	Glyoxylate Shunt (X1.5)	3	0	**0**	3	0	+3	1.5	248.9	**83.0**
	TOTAL	5	0	**−6**	5	6	−1	1.5	1.9	**0.4**
R-S	Glutamate Synthesis (X2)	2	−2	**0**	2	2	0	0	0.0	**0.0**
	EMC (X1)	2	+2	**−1**	1	2	−1	2	23.2	**11.6**
	Glyoxylate Utilization (X1)	1	0	**0**	1	0	+1	0	42.5	**42.5**
	TOTAL	5	0	**−1**	4	4	0	2	65.6	**13.1**

3.8. Carbon recovery following glutamate synthesis

The true advantage of the EMC pathway might occur specifically under saline conditions. Glutamate synthesis plays a key role in maintaining osmotic and ionic homeostasis, a behavior reflected in the overexpression of GDH in R-S (Fig. 4).

During glutamate biosynthesis, decarboxylation at the isocitrate to α-ketoglutarate step results in the loss of CO_2. The EMC pathway offers a strategy to reincorporate this lost carbon without resorting to the energetically expensive CBB cycle, which consumes 2 NADPH and 3 ATP per CO_2 fixed.

For the synthesis of two glutamate molecules, a single turn of the EMC cycle (along with further glyoxylate assimilation) can compensate for this carbon loss using 3 acetyl-CoA and generating a net redox output of 13.12 kJ/mol (Table 1). In contrast, achieving carbon compensation through the CBB cycle would require 4 NADPH and 6 ATP. If the glyoxylate shunt were used to metabolize the 3 acetyl-CoA equivalents consumed by EMC, the net redox output would be almost zero, with 6 ATP consumed.

This analysis challenges the conventional view of EMC as merely an electron sink. Instead, under saline conditions, EMC may function as a source of reductive power and contribute to the generation of proton motive force, enabling both carbon recovery and redox balance during osmoadaptative glutamate overproduction. The enhanced reducing power (NADPH and $FADH_2$) generated by EMC in R-S likely plays a crucial role in mitigating osmotic stress (supporting the biosynthesis and transport of the compatible solutes) and maintaining redox balance. Moreover, the increased availability of reducing equivalents likely contributes to the high levels of PHA accumulation observed in R-S (Fig. 1). PHA granules, beyond their function as carbon and energy reserves, have been proposed to act as electron sinks to balance redox states within cells (Fradinho et al., 2016).

As *Cereibacter* lacks the glyoxylate cycle enzyme ICL (Alber et al., 2006), EMC is the only option for carbon assimilation. Thus, the observed metabolic shift in R-S might be a consequence of *Cereibacter* dominance, rather than a direct effect of salinity itself, although salinity likely acted as the selective pressure favoring this genus. This hypothesis deserves more research effort in the future to obtain related biochemical evidence. Such data could be obtained from NAD(P)H/$FADH_2$ quantification, metabolomics or isotopic flux analysis in dedicated assays.

4. Conclusions

A mixed microbial culture of PPB was adapted from non-saline (R-NS) to saline conditions (35 g NaCl/L, R-S), exhibiting higher PHA accumulation (41.7 vs. 11.0 dw%), mainly as PHB. Major microbial activities differences were found between both reactors, R-NS was enriched in *Rhodopseudomonas*, and R-S in *Cereibacter*.

Correspondingly, metaproteomic analysis of carbon assimilation enzymes revealed two different metabolic strategies. R-NS activated the glyoxylate cycle, whereas R-S relied on the EMC pathway. This more complex route in R-S reintroduces carbon lost through decarboxylation during glutamate synthesis, producing reducing power while carboxylating, challenging the concept of EMC as merely electron sink.

Thus, glutamate became a key intermediate in both carbon and redox balance, affected by the osmotic response. These findings suggest that supplementing glutamate as nitrogen source could enhance reducing power availability, ultimately improving PHA synthesis in PPB cultures.

CRediT authorship contribution statement

Jose Ramon Lorenzo-Llarena: Writing – review & editing, Writing – original draft, Visualization, Validation, Methodology, Investigation, Formal analysis, Data curation, Conceptualization. **Alba Trueba-Santiso:** Writing – review & editing, Validation, Methodology, Investigation, Formal analysis, Data curation. **Anuska Mosquera-Corral:** Writing – review & editing, Validation, Supervision, Project administration, Funding acquisition, Conceptualization. **Alba Pedrouso:** Writing – review & editing, Writing – original draft, Validation, Supervision, Project administration, Methodology, Formal analysis, Data curation, Conceptualization.

Declaration of competing interest

The authors declare that they have no known competing financial interests or personal relationships that could have appeared to influence the work reported in this paper.

Acknowledgments

This work was supported by the Spanish Government (MICIU/AEI/10.13039/501100011033) through the ECOPOLYVER (PID2020-112550RB-C21) project. José Ramón Lorenzo-Llarena is grateful to the Ministry of Science, Innovation, and Universities (Spain) for the FPU

Grant (FPU-021/05797). Alba Pedrouso acknowledges the Xunta de Galicia (Spain) for her postdoctoral fellowships (ED481B-2021-041 and ED481D-2024-010). The authors are part of a Galician Competitive Research Group (GRC ED431C2021/37), a program co-funded by FEDER (UE).

Appendix A. Supplementary data

Supplementary data to this article can be found online at https://doi.org/10.1016/j.biortech.2025.133171.

Data availability

Data will be made available on request.

References

Alber, B.E., Spanheimer, R., Ebenau-Jehle, C., Fuchs, G., 2006. Study of an alternate glyoxylate cycle for acetate assimilation by Rhodobacter sphaeroides. Mol. Microbiol. 61, 297–309. https://doi.org/10.1111/J.1365-2958.2006.05238.X.

American Public Health Association, American Water Works Association, Water Environment Federation, 2023. Standard Methods for the Examination of Water and Wastewater , 24th Ed. ed. Washington DC.

Bayon-Vicente, G., Wattiez, R., Leroy, B., 2020. Global proteomic analysis reveals high light intensity adaptation strategies and polyhydroxyalkanoate production in rhodospirillum rubrum cultivated with acetate as carbon source. Front. Microbiol. 11, 492393. https://doi.org/10.3389/FMICB.2020.00464/BIBTEX.

Berg, J.M., Gregory, J.G.J.J.J.L., Stryer, L., 2023. Biochemistry (International Edition) Berg, Jeremy M., Gregory, J.G., Jr., Hines, J., Tymoczko, J.L., Stryer, L.

Bower, C.E., Holm-Hansen, T., 1980. A salicylate–hypochlorite method for determining ammonia in seawater. Can. J. Fish. Aquat. Sci. 37, 794–798. https://doi.org/10.1139/f80-106.

Capson-Tojo, G., Batstone, D.J., Grassino, M., Vlaeminck, S.E., Puyol, D., Verstraete, W., Kleerebezem, R., Oehmen, A., Ghimire, A., Pikaar, I., Lema, J.M., Hülsen, T., 2020. Purple phototrophic bacteria for resource recovery: challenges and opportunities. Biotechnol. Adv. https://doi.org/10.1016/j.biotechadv.2020.107567.

Carlozzi, P., Di Lorenzo, T., Ghanotakis, D.F., Touloupakis, E., 2020. Effects of pH, temperature and salinity on P3HB synthesis culturing the marine Rhodovulum sulfidophilum DSM-1374. Appl. Microbiol. Biotechnol. 104, 2007–2015. https://doi.org/10.1007/s00253-020-10352-1.

Carvalho, J.M., Marreiros, B.C., Gaudêncio, S.P., Fradinho, J.C., 2025. Valorization of organic rich saline streams by purple phototrophic bacteria mixed cultures through polyhydroxyalkanoates production. Bioresour. Technol. 435, 132924. https://doi.org/10.1016/J.BIORTECH.2025.132924.

Carvalho, J.M., Marreiros, B.C., Reis, M.A.M., 2022. Polyhydroxyalkanoates production by mixed microbial culture under high salinity. Sustainability (Switzerland) 14, 1346. https://doi.org/10.3390/SU14031346/S1.

Cerruti, M., 2022. Light intensity defines growth and photopigment content of a mixed culture of purple phototrophic bacteria. Front. Microbiol. 13. https://doi.org/10.3389/fmicb.2022.1014695.

Dat, L.T., Xuan, L.N.T., Nhan, T.C., Quang, L.T., Khuong, N.Q., 2024. Isolating, selecting, and identifying Na+, H+, Al3+, Fe2+, Mn2+-resistant purple non-sulfur bacteria solubilizing insoluble phosphorus compounds from salt-contaminated acid sulfate soil derived from rice-shrimp system. Aust. J. Crop Sci. 18, 192–199. https://doi.org/10.21475/ajcs.24.18.04.PNE-07.

Eprintsev, A.T., Klimova, M.A., Falaleeva, M.I., Kompantseva, E.I., 2008. Regulation of carbon flows in the tricarboxylic acid cycle-glyoxylate bypass system in Rhodopseudomonas palustris under different growth conditions. Microbiology (NY) 77, 132–136. https://doi.org/10.1134/S0026261708020021.

Erb, T.J., Berg, I.A., Brecht, V., Müller, M., Fuchs, G., Alber, B.E., 2007. Synthesis of C5-dicarboxylic acids from C2-units involving crotonyl-CoA carboxylase/reductase: the ethylmalonyl-CoA pathway. PNAS 104, 10631–10636. https://doi.org/10.1073/PNAS.0702791104/SUPPL_FILE/02791FIG7B.PDF.

Fradinho, J.C., Reis, M.A.M., Oehmen, A., 2016. Beyond feast and famine: Selecting a PHA accumulating photosynthetic mixed culture in a permanent feast regime. Water Res. 105, 421–428. https://doi.org/10.1016/j.watres.2016.09.022.

Hiraishi, A., Ueda, Y., 1994. Rhodoplanes gen. nov., a new genus of phototrophic bacteria including Rhodopseudomonas rosea as Rhodoplanes roseus comb. nov. and Rhodoplanes elegans sp. nov. Int. J. Syst. Bacteriol. 44, 665–673. https://doi.org/10.1099/00207713-44-4-665/CITE/REFWORKS.

Hördt, A., López, M.G., Meier-Kolthoff, J.P., Schleuning, M., Weinhold, L.M., Tindall, B. J., Gronow, S., Kyrpides, N.C., Woyke, T., Göker, M., 2020. Analysis of 1,000+ type-strain genomes substantially improves taxonomic classification of alphaproteobacteria. Front. Microbiol. 11, 493139. https://doi.org/10.3389/FMICB.2020.00468/BIBTEX.

Hülsen, T., Hsieh, K., Batstone, D.J., 2019. Saline wastewater treatment with purple phototrophic bacteria. Water Res. 160, 259–267. https://doi.org/10.1016/j.watres.2019.05.060.

Hunter, C.N., Daldal, F., Thurnauer, M.C., Beatty, J.T., 2009. The Purple Phototrophic Bacteria, 1st ed. Springer, Dordrecht.

Imhoff, J.F., 2001. True marine and halophilic anoxygenic phototrophic bacteria. Arch. Microbiol. 176, 243–254. https://doi.org/10.1007/S002030100326/METRICS.

Imhoff, J.F., Rahn, T., Künzel, S., Keller, A., Neulinger, S.C., 2020. Osmotic Adaptation and Compatible Solute Biosynthesis of Phototrophic Bacteria as Revealed from Genome Analyses. Microorganisms 2021, Vol. 9, Page 46 9, 46. doi:10.3390/MICROORGANISMS9010046.

Imhoff, J.F., Truper, H.G., Pfennig, N., 1984. Rearrangement of the species and genera of the phototrophic "purple nonsulfur bacteria. Int. J. Syst. Bacteriol. 34, 340–343. https://doi.org/10.1099/00207713-34-3-340/CITE/REFWORKS.

Klaysubun, C., Chaichana, N., Suwannasin, S., Singkhamanan, K., Yaikhan, T., Kantachote, D., Pomwised, R., Wonglapsuwan, M., Surachat, K., 2024. Genomic characterization of probiotic purple nonsulfur bacteria cereibacter sphaeroides strains S3W10 and SS15: implications for enhanced shrimp aquaculture. Life 14, 1691. https://doi.org/10.3390/LIFE14121691/S1.

Kleiner, M., 2019. Metaproteomics: Much More than Measuring Gene Expression in Microbial Communities. mSystems 4. doi:10.1128/msystems.00115-19.

Liu, X., Li, D., Yan, X., Zhang, Z., Zheng, S., i, J.Z., Wu, F., Li, F., Chen, G.-Q., 2022. Rapid quantification of polyhydroxyalkanoates accumulated in living cells based on green fluorescence protein labeled phasin: The qPHA method. bioRxiv 2022.03.02.482659. doi:10.1101/2022.03.02.482659.

Ma, B., Zhang, K., Hendrie, C., Liang, C., Li, M., Doherty-Kirby, A., Lajoie, G., 2003. PEAKS: powerful software for peptide de novo sequencing by tandem mass spectrometry. Rapid Commun. Mass Spectrom. 17, 2337–2342. https://doi.org/10.1002/RCM.1196.

Maehara, A., Taguchi, S., Nishiyama, T., Yamane, T., Doi, Y., 2002. A repressor protein, PhaR, regulates polyhydroxyalkanoate (PHA) synthesis via its direct interaction with PHA. J. Bacteriol. 184, 3992. https://doi.org/10.1128/JB.184.14.3992-4002.2002.

McKinlay, J.B., Harwood, C.S., 2010. Carbon dioxide fixation as a central redox cofactor recycling mechanism in bacteria. PNAS 107, 11669–11675. https://doi.org/10.1073/PNAS.1006175107/SUPPL_FILE/ST07.DOC.

Mosquera-Corral, A., Val del Río, Á., Campos, J.L., 2021. Treatment and valorisation of saline wastewater: Principles and practice. Treatment and Valorisation of Saline Wastewater: Principles and Practice 1–202. https://doi.org/10.2166/9781789060645.

Mugnai, G., Bernabò, L., Daly, G., Corneli, E., Adessi, A., 2025. Photofermentative production of poly-β-hydroxybutyrate (PHB) by purple non-sulfur bacteria using olive oil by-products. Bioresour Bioprocess 12, 1–15. https://doi.org/10.1186/S40643-025-00856-X/FIGURES/5.

Niederman, R.A., 2006. Structure, Function and Formation of Bacterial Intracytoplasmic Membranes. In: Complex Intracellular Structures in Prokaryotes. Springer, Berlin, Heidelberg, pp. 193–227. https://doi.org/10.1007/7171_025.

Oliveira, C.S.S., Silva, C.E., Carvalho, G., Reis, M.A., 2017. Strategies for efficiently selecting PHA producing mixed microbial cultures using complex feedstocks: Feast and famine regime and uncoupled carbon and nitrogen availabilities. N. Biotechnol. 37, 69–79. https://doi.org/10.1016/J.NBT.2016.10.008.

Ollivier, B., Caumette, P., Garcia, J.L., Mah, R.A., 1994. Anaerobic bacteria from hypersaline environments. Microbiol. Rev. 58, 27–38. https://doi.org/10.1128/MR.58.1.27-38.1994.

Ormerod, J.G., Ormerod, K.S., Gest, H., 1961. Light-dependent utilization of organic compounds and photoproduction of molecular hydrogen by photosynthetic bacteria; relationships with nitrogen metabolism. Arch. Biochem. Biophys. 94, 449–463. https://doi.org/10.1016/0003-9861(61)90073-X.

Pérez-Arellano, I., Carmona-Álvarez, F., Martínez, A.I., Rodríguez-Díaz, J., Cervera, J., 2010. Pyrroline-5-carboxylate synthase and proline biosynthesis: from osmotolerance to rare metabolic disease. Protein Sci. 19, 372–382. https://doi.org/10.1002/PRO.340.

Perez-Riverol, Y., Bandla, C., Kundu, D.J., Kamatchinathan, S., Bai, J., Hewapathirana, S., John, N.S., Prakash, A., Walzer, M., Wang, S., Vizcaíno, J.A., 2025. The PRIDE database at 20 years: 2025 update. Nucleic Acids Res. 53, D543–D553. https://doi.org/10.1093/NAR/GKAE1011.

Petushkova, E., Mayorova, E., Tsygankov, A., 2021. TCA Cycle Replenishing Pathways in Photosynthetic Purple Non-Sulfur Bacteria Growing with Acetate. Life 2021, Vol. 11, Page 711 11, 711. doi:10.3390/LIFE11070711.

Petushkova, E.P., Tsygankov, A.A., 2017. Acetate metabolism in the purple non-sulfur bacterium Rhodobacter capsulatus. Biochem. Mosc. 82, 587–605. https://doi.org/10.1134/S0006297917050078/METRICS.

Quiton-Tapia, S., Trueba-Santiso, A., Garrido, J.M., Suarez, S., Omil, F., 2023. Metalloenzymes play major roles to achieve high-rate nitrogen removal in N-damo communities: Lessons from metaproteomics. Bioresour. Technol. 385, 129476. https://doi.org/10.1016/J.BIORTECH.2023.129476.

Rajendran, N., Han, J., 2022. Techno-economic analysis of food waste valorization for integrated production of polyhydroxyalkanoates and biofuels. Bioresour. Technol. 348, 126796. https://doi.org/10.1016/J.BIORTECH.2022.126796.

Sagong, H.Y., Son, H.F., Choi, S.Y., Lee, S.Y., Kim, K.J., 2018. Structural Insights into Polyhydroxyalkanoates Biosynthesis. Trends Biochem. Sci 43, 790–805. https://doi.org/10.1016/J.TIBS.2018.08.005.

Shi, X., Zou, Y., Zhang, Y., Ding, G., Xiao, Y., Lin, S., Chen, J., 2024. Salinity decline promotes growth and harmful blooms of a toxic alga by diverting carbon flow. Glob. Chang. Biol. 30, e17348. https://doi.org/10.1111/GCB.17348.

Slater, S., Houmiel, K.L., Tran, M., Mitsky, T.A., Taylor, N.B., Padgette, S.R., Gruys, K.J., 1998. Multiple β-ketothiolases mediate poly(β-Hydroxyalkanoate) copolymer synthesis in ralstonia eutropha. J. Bacteriol. 180, 1979. https://doi.org/10.1128/JB.180.8.1979-1987.1998.

Smolders, G.J.F., van der Meij, J., van Loosdrecht, M.C.M., Heijnen, J.J., 1994. Stoichiometric model of the aerobic metabolism of the biological phosphorus

removal process. Biotechnol. Bioeng. 44, 837–848. https://doi.org/10.1002/bit.260440709.

Soto, M., Veiga, M.C., Méndez, R., Lema, J.M., 1989. Semi-micro C.O.D. determination method for high-salinity wastewater. Environ. Technol. Lett. 10, 541–548. https://doi.org/10.1080/09593338909384770.

Tammam, S.D., Rochet, J.C., Fraser, M.E., 2007. Identification of the cysteine residue exposed by the conformational change in pig heart succinyl-CoA:3-ketoacid coenzyme A transferase on binding coenzyme A. Biochemistry 46, 10852–10863. https://doi.org/10.1021/BI700828H/SUPPL_FILE/BI700828H-FILE002.PDF.

Tsuzuki, M., Moskvin, O.V., Kuribayashi, M., Sato, K., Retamal, S., Abo, M., Zeilstra-Ryalls, J., Gomelsky, M., 2011. Salt stress-induced changes in the transcriptome, compatible solutes, and membrane lipids in the facultatively phototrophic bacterium Rhodobacter sphaeroides. Appl. Environ. Microbiol. 77, 7551–7559. https://doi.org/10.1128/AEM.05463-11/SUPPL_FILE/AEM05463-11_SUP03.PDF.

Xu, X., Abo, M., Okubo, A., Yamazaki, S., 1998. Trehalose as osmoprotectant in Rhodobacter sphaeroides f. sp. denitrificans IL106. Biosci. Biotech. Bioch. 62, 334–337. https://doi.org/10.1271/BBB.62.334.

Yuan, Q., Sparling, R., Oleszkiewicz, J., 2015. Polyhydroxybutyrate production from municipal wastewater activated sludge with different carbon sources. Air Soil Water Res. 2015, 53–58.

Zhao, Y., Lin, Y.H., 2010. Whole-cell protein identification using the concept of unique peptides. Genomics Proteomics Bioinformatics 8, 33. https://doi.org/10.1016/S1672-0229(10)60004-6.